Invited Paper

The Development of broadband millimeter-wave and terahertz gyro-TWAs

W. He [1*], L. Zhang [2], C. R. Donaldson [2], H. Yin [2], K. Ronald [2], A. W. Cross [2] and A. D. R. Phelps [2]
[1] College of Electronics and Information Engineering, Shenzhen University, Shenzhen, China
[2] SUPA, Department of Physics, University of Strathclyde, Glasgow, G4 0NG, Scotland, UK
[*1] Email: wenlong.he@szu.edu.cn

(Received 02 March 2020)

Abstract: The gyrotron travelling wave tube amplifiers (gyro-TWAs) presented in this paper can operate with high efficiency (30%), huge powers and wide bandwidths at high frequencies that no other amplifier can provide. In principle, this is a technology that can be scaled to >1 THz and operate with 20% bandwidths. Resonant coupling of two dispersive waveguide modes in a helically corrugated interaction region (HCIR) can give rise to a non-dispersive eigenwave over a wide frequency band. The synchronism between the ideal wave and an electron cyclotron mode, either fundamental or harmonic, of a large orbit electron beam contributes to the broadband amplification. An electron beam of 55 *keV*, 1.5 *A* with a velocity pitch angle of ~1 generated by a thermionic cusp gun is used in our 100 *GHz* gyro-TWA experiment, which achieves an unsaturated output power of 3.4 *kW* and gain of 36–38 *dB*. The design and experimental results of the many components making the gyro-TWA will be presented individually and then the whole system will be introduced. The amplification of a swept signal by the W-band gyro-TWA is demonstrated showing its capabilities in the field of telecommunications. Furthermore, the design studies of a cusp electron gun in the triode configuration and the realization of a 3-fold HCIR operating at 372 *GHz* will also be displayed.

Keywords: Gyro-TWA, Corrugated waveguide, Helically corrugated interaction region, Broadband amplification, Gyro-devices.

doi:

1. Introduction

Generations of high-power sub-millimeter and terahertz (THz) radiation have drawn great interest in the last few decades due to their wide applications, such as communications, remote sensing, plasma heating, electron spin resonance, dynamic nuclear polarization-enhanced nuclear magnetic resonance, and others. As the operating wavelength moves towards the millimeter range, conventional microwave sources, such as travelling wave tubes and klystrons, become greatly limited by their power capability, due to a low current density, excessive heat load, small dimensions (especially in the interaction circuit) and the associated machining difficulties. Gyro-devices are based on the cyclotron resonance maser (CRM) instability [1] and they have a fast

wave interaction. The electromagnetic field interacts with the transverse energy of the electron beam. By operating at higher modes, gyrotrons can generate radiation close to the THz range with larger dimensions when compared with the conventional microwave sources.

The gyrotron traveling wave amplifier (gyro-TWA) is a part of the gyro-family. As an amplifier, it has many advantages in applications compared with gyro-oscillators. A higher-order mode operation brings many benefits such as a larger power capability, operation at discrete frequencies and higher interaction efficiency. However, mode competition is still a challenge that requires substantial effort to solve. Nevertheless, applications such as communications and radar can be greatly enhanced if broadband amplification can be achieved. The high-power broadband amplification is also very attractive for spectroscopy in the fields of bioscience and medical science.

Gyro-devices with a smooth interaction waveguide have a hyperbolic dispersion curve. To achieve wide bandwidth amplification, the gyro-amplifiers must operate far from the cut-off as the group velocity has large variation near the cut-off and less far from the cut-off. However, the group velocity in the large axial wavenumber region is close to the speed of light. The gyrating electron beam is required to have large energy and a low spread in the transverse-to-axial velocity ratio (pitch alpha), which makes it unattractive to be used in the gyro-TWAs interaction circuit. A helically corrugated interaction region (HCIR) was proposed in 1998 [2], since then theoretical, numerical, and experimental studies were carried out to explore and validate its applications. The HCIR has very interesting features that it is able to couple any two modes in a circular waveguide to generate new eigenmodes. The details of the mode coupling can be referred to in the following section. The HCIR has been successfully used in gyrotron backward wave oscillators (gyro-BWOs) [3, 4], gyro-TWAs [5-7], microwave pulse compressors [8-10], and as microwave undulators for free-electron lasers [11, 12].

This paper summarizes the research work of high-power, broadband millimeter-wave and THz gyro-TWAs based on HCIRs conducted by the authors. There are gyro-TWAs with other interaction circuits that have been developed and have achieved great performance [13-16], whilst this paper concentrates on the gyro-TWA using the HCIR. At W-band the gyro-TWA achieved an unsaturated output power of 3.4 *kW* and a gain of 36-38 *dB* in the frequency range of 90-96 *GHz* [7]. Further experiments demonstrated its potential application in communications [7]. A summary of the design of the individual components in the gyro-TWA is also presented in this paper. Besides the HCIR, another novelty of the design is the use of a large-orbit beam which was generated from a cusp electron gun. The large-orbit beam has the advantage of mode selection to reduce the mode competition, which allows the gyro-TWA to operate at the second harmonic of the cyclotron frequency, as required by the chosen interaction region. Therefore, this allows a reduction in the required magnetic field strength by a factor of 2. Currently, a THz gyro-TWA has been developed and its progress is also introduced in the last section of this paper.

2. The w-band gyro-twa system and individual components

In the past decades, gyro-TWAs using the HCIR in different frequency bands have been successfully developed, such as at X-band [5, 6], Ka-band [17, 18] and W-band [7, 19]. The schematic drawing of the W-band gyro-TWA is shown in Fig. 1. Critical components include the electron gun (2), magnetic coils (1, 6), input coupling system (3-4), elliptical polarizer (5), HCIR (7), output taper and an output launcher with microwave window (8). A diode with an annular electron emitter was used to form the electron beam which then propagated through a magnetic field cusp, just after the cathode, produced by a combination of two opposing magnetic fields initiating cyclotron motion around the longitudinal axis of the system. The magnetic system served to confine and transport the electron beam, as well as to provide the required magnetic field strength in the interaction region. The input coupling system enabled the low power millimeter-wave signal, generated by a solid-state source, to couple into the interaction region.

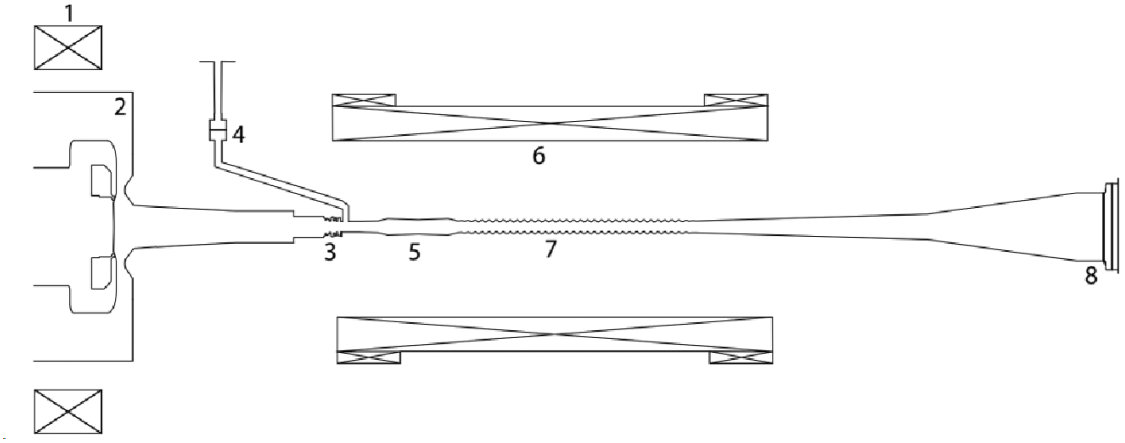

Fig. 1 The schematic of the W-band gyro-TWA.

The optimal performance of the gyro-TWA requires its individual components to meet strict metrics. The design of the cusp electron gun geometry is made to match the magnetic field profile to achieve the required alpha pitch with a minimum alpha spread. The input and output coupling systems must be designed with maximum transmission coefficients over the designed frequency band and minimal reflections to avoid parasitic oscillations. The input coupling system has the rectangular waveguide TE_{10} mode as its input, to match the output from the solid-state source, it is then converted to the circular TE_{11} mode before the entrance to the HCIR. To meet the requirements of many applications the output mode is desired to be a high purity Gaussian. Therefore, the output launcher, incorporating the microwave window, will also act as a mode converter to achieve the designed field profile. In the following sections, the design and measurement of each component are presented in detail.

(a) Helically corrugated interaction region

The HCIR has an idealized dispersion characteristic that acts to improve the gyro-TWAs bandwidth and reduce the effect of electron beam velocity spread while maintaining a high interaction efficiency. It has a helical inner profile described by

$$r(\theta, z)=R_0+R_1\cos(m_B\theta - 2\pi z/d) \quad (1)$$

where R_0 is the mean radius of the circular waveguide, R_1 is the corrugation depth, m_B is the fold number, and d is the axial period of the corrugation. Fig. 2 shows its inner surface. The azimuthal and axial periodicity allows coupling of two modes in the circular waveguide to generate new eigenwaves, as shown in Fig. 3.

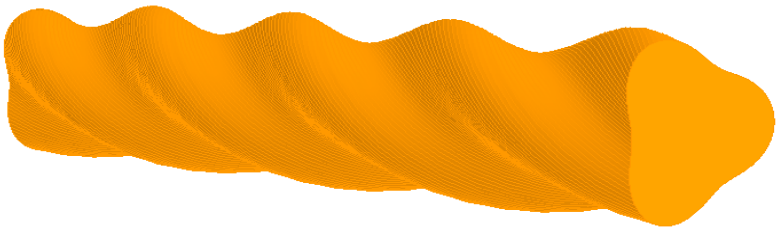

Fig. 2 The inner surface of the helically corrugated interaction region

One of the eigenwaves has nearly constant group velocity over a large range of frequencies and is suitable for the beam-wave interaction. By careful control of the dimensions of the HCIR, different "ideal" dispersions can be achieved for different frequencies ranges. For example, the gyro-TWA requires a nearly constant group velocity over a wide frequency range; the microwave compressor requires a swept group velocity over a wide frequency range; the microwave undulator requires a specific mode coupling at a certain frequency.

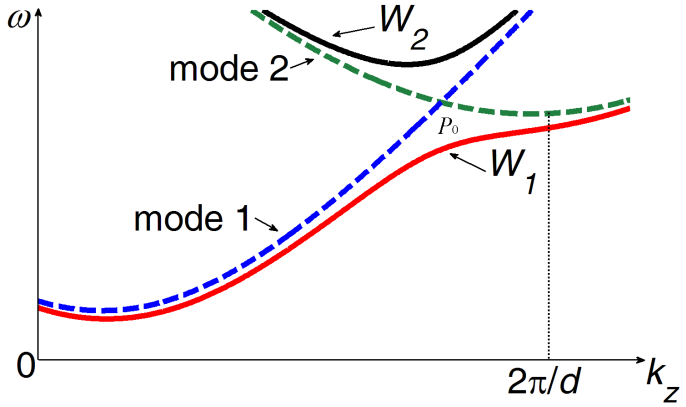

Fig. 3 The mode coupling in the HCIR

To find the optimal dispersion curve that can achieve a broad bandwidth amplification, it is important to calculate the dispersion relation and the field distribution inside the HCIR accurately.

Different methods have been developed, including the 1D coupled wave theory based on the method of perturbation [20, 21], 2D finite-difference time-domain method (FDTD) / finite element method (FEM) eigensolver based on helicoidal coordinate transform [22], and the full 3D FDTD transient solver, or FEM eigenmode solver [23]. The 1D coupled wave theory based on the method of perturbation is the simplest and fastest method to calculate the dispersion curves. It assumes that the change in the cross-section is small ($R_1 << R_0$) and can be treated as a first-order derivative of a regular circular waveguide. When the corrugation depth is less than 15% of the mean waveguide radius, the coupled wave theory gives reasonably accurate results. Based on the perturbation theory, the small-signal gain equation can be derived to predict the performance of the gyro-TWA based on the HCIR. The HCIR can also be regarded as a type of twisted waveguide. A helicoidal coordinate transform can be used to convert the twisted waveguide into a straight uniform waveguide, thus downgrading the 3D problem into a 2D one, which can reduce the computing time by an order compared with the 3D method while maintaining high accuracy. Its drawback is that it is not straightforward to interpolate the 2D field pattern back to 3D due to the twisted coordinate system. The 3D simulations, either by a FDTD solver or a FEM eigensolver, require long simulation time and large computing resources, so they are suitable to verify the 1D and 2D simulation results.

As an interaction region, the HCIR has the advantages of broadband amplification up to 20%. With the optimal design, the eigenwave at small axial wavenumbers has near-constant group velocity, which makes it less sensitive to the electron beam velocity spread. By using a 3-fold HCIR, its operating mode is coupled by TE_{21} and the spatial harmonic of TE_{11} mode. The major interaction mode is TE_{21}, therefore, the second harmonic operation reduces the requirement of the magnetic field strength. For the W-band gyro-TWA, the simulated and measured dispersion curves are shown in Fig. 4. The small-signal gain was calculated using the normalized equation [5]

$$\begin{aligned}&[(k_{zn}^2-2f_n)(k_{zn}+\Delta_g-f_n/h_0)+2\sigma^2/h_0][k_{zn}-(f_n-\Delta_H)/\beta_{z0}]^2\\&=C^3(k_{zn}+\Delta_g-f_n/h_0)\left\{1+\frac{2s}{\alpha_0^{\ 2}\beta_{z0}}[k_{zn}-(f_n-\Delta_H)/\beta_{z0}]\right\}\end{aligned} \tag{2}$$

where α_0 and β_{z0} are the beam initial alpha pitch and relative velocity in longitudinal direction respectively. f_n and k_{zn} are the normalized frequency and axial wavenumber. Δ_g and Δ_H are the geometric mismatches of the HCIR and the normalized detuning between the operating eigenwave and the electron cyclotron mode. s is the harmonic number of the electron cyclotron mode. The calculated linear gain of the designed interaction circuit with an electron beam voltage of 55 *kV* and an alpha pitch value of 1.0 was about 40 *dB* over the frequency range of 90 -100 *GHz*.

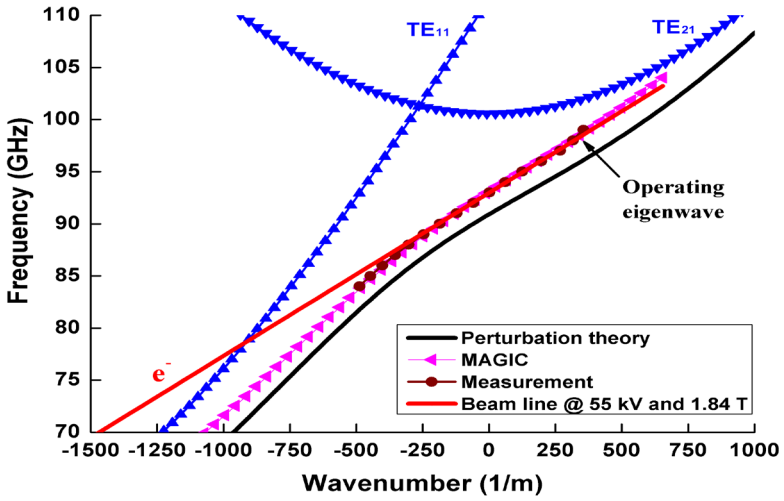

Fig. 4 The dispersion curve of the W-band gyro-TWA

(b) Cusp electron gun

The electron beam source is determined by the interaction region used, in this case, a large-orbit beam is required.

This could be achieved through, for instance, a Piece-type beam traveling through a magnetic kicker. However, the cusp electron gun presents many benefits; an annual beam profile, controllable beam alpha and a mode selective beam quality. Initially, transport of an electron beam through opposing magnetic fields (the so-called "magnetic cusp") was investigated in the 1960s [24] for plasma-heating applications. Schmidt described the effects on electrons that passed through the cusp region, namely that they gained azimuthal rotation around the central axis of symmetry due to conservation of the electron canonical momentum[25, 26]. Building on this initial study cusp-based electron-beam sources started to be reported [27, 28]. Culminating in the "state-of-the-art" cusp electron gun in 2000 by Northrop Grumman [29] with a 70 *kV*, 3.5 *A* and 1.5 alpha electron beam with an axial velocity spread of 5% at a magnetic field of ~0.25 *T*. The first microwave source using a cusp electron gun was reported in 1983 using a magnetron [30]. Those earlier studies concentrated on a system with a cusp located after, or in, the anode region. However, the design in this gyro-TWA a smooth cusp just formed in front of the cathode. This provides some advantages, namely that the electron has not yet fully accelerated, and the required magnetic field which used to achieve a large orbit beam can be much small, so the velocity spread can also be therefore smaller. Since its inception cusp electron guns have gained popularity and have been used in many microwave and mm-wave sources, due to the attractive qualities such beams had, as discussed above.

The particle-in-cell code MAGIC was used to simulate and optimize the trajectories of the cusp electron gun. Its basic geometry was derived from the Pierce-type gun. However, its design

is much more complicated compared with a Pierce gun. Although the approximated value of some key parameters, such as the radius of the emitter, magnetic field strengths at the cathode and the interaction region, can be derived from the analytical equations, it is hard to predict the trajectories in the compression region. So far, there is not a synthesis method available to achieve a simple design. At the same time, to achieve a small alpha spread, which is required for effective beam-wave interaction, the electric field between the cathode and anode needs to match with the magnetic field profile. Further researches have found that it is possible to decouple the design of the electric field and the magnetic field. There exists a range of magnetic field profiles, where an electric field distribution inside the electron gun can be designed and optimized to achieve optimal results. The design detail of the cusp electron gun can be referred to in papers [31-33]. Fig. 5 shows the optimal electron gun geometry as well as the beam trajectories.

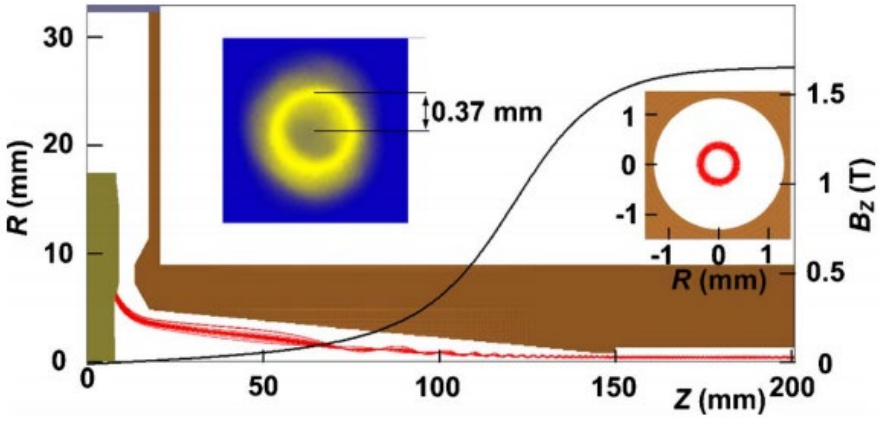

Fig. 5 The simulated electron beam trajectories of the cusp electron gun.

In the cusp electron gun experimental measurement, a double cable Blumlein which could output a ~380 *ns*, 40-60 *kV* pulse was used to drive the cusp gun. The beam quality was optimized in the beam voltage range which could be used to demonstrate the versatility of the gyro-TWA in operating at different parameter sets. The beam voltage was measured using a two-stage voltage divider made from metal film resisters. The emitted current was measured with a Rogowski coil located in the earth line between the anode and the cable Blumlein and the beam current by a Faraday cup. The beam cross-sectional shape and dimensions were recorded by a phosphor scintillator plate and digital camera system after the Faraday cup was removed. The scintillator, a round transparent disk coated with a thin layer of phosphor, produces visible light when electrons impact on the surface. A thin titanium disk was placed before the scintillator to reduce the impact energy of the beam. The scintillator disk was located at 10.5 *cm* from the window (marked as position Z_1) to match with the focal length of the camera, at this position the magnetic field tailed off to 90% of the cavity B-field. Typical traces of beam voltage and beam current are shown in Fig. 6 when operating at 40 *kV*. The emitted current from the cathode could be varied from 0 to 1.6 *A* by increasing the operating temperature of the cathode, at the applied beam voltage of 40 *kV*. Further increase in the temperature did not result in an increase in the beam current. This indicated that the operation of the cathode had become space-charge limited.

When the cavity B-field was 1.82 *T*, about 96% of this current reached the Faraday cup. A typical scintillator image, after the optical noise was removed, is shown in the inset of Fig. 5. The image shows clearly that an axis-encircling electron beam was generated. For this measurement, at a cavity B-field of 1.64 *T*, the annular beam was measured to have an average radius of ~0.37 *mm*. In the calculation, the corresponding alpha value was about 1.34 at the position of Z_1. This corresponded to an alpha value of 1.56 at the entrance of the interaction region (marked as the position of Z_2).

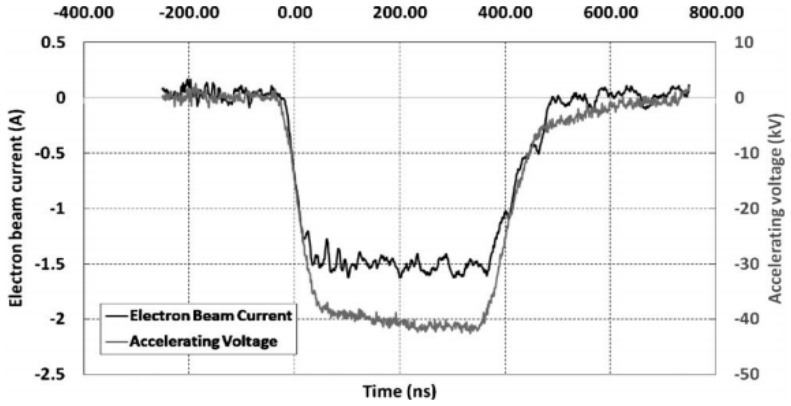

Fig. 6 The measured beam voltage and current.

By adjusting the reverse coil current the magnetic field at the cathode and hence the value of the velocity ratio of the beam in the cavity could be controlled. At the cavity magnetic field strength of 1.64 *T*, the velocity ratio at position Z_2 as a function of cathode B-field was measured and is shown in Fig. 7. For comparison of the simulated alpha at Z_1 and Z_2 as well as analytically calculated value at Z_2 are also shown in the same figure. From the diagram, the measured alpha value had the same trend and a good agreement with both the numerical simulated and analytically calculated values. However investigation at higher alphas was limited by the capability of the existing power supply.

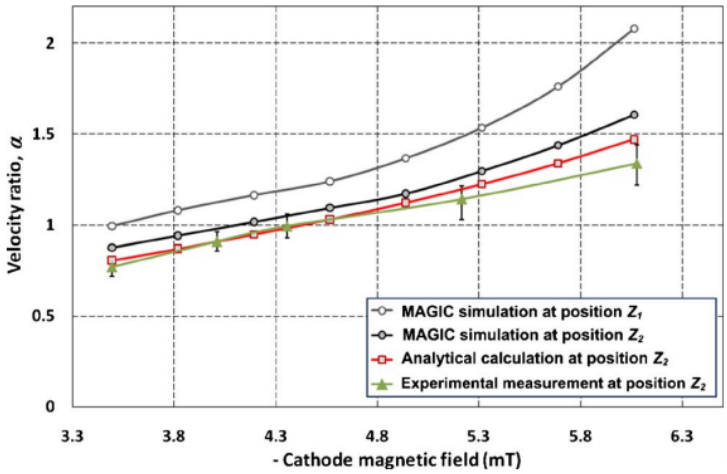

Fig. 7 The simulated and measured cusp gun results for the W-band gyro-TWA.

(c) Input coupling system

The input coupling system not only separated the atmosphere from the ultra-high vacuum (UHV) inside the gyro-TWA but also ensured efficient mode coupling between the input modes from the TE_{10} mode in a rectangular waveguide to the TE_{11} mode in the circular waveguide. If the losses or reflection from the input coupling system is too high then there is a drop in the output power from the gyro-TWA requiring a higher power from the solid-state input source, which is either costly or may not be possible. Undesired oscillations may also occur if the reflection sufficiently large.

The input coupling system consisted of a microwave window, a waveguide bend and a mode converter [34-37]. A pillbox window was used to seal the vacuum. It was convenient as it could connect to the solid-state source and directly use the rectangular TE_{10} mode as its input and output. Further advantages of the pillbox window included a relatively simple geometry, being able to be conveniently modeled through the mode-matching method, and a balanced performance between bandwidth and transmission. To improve the bandwidth performance, an impedance matching section was added between the rectangular waveguides. Also, the pillbox window mechanical structure was designed with a custom CF-like knife-edge on its UHV end for it to be demountable and able to be used in other applications. The measurement of the pillbox window showed it was able to hold a vacuum to the 10^{-9} mBar level while achieving a better than -15 *dB* reflection in the required frequency range of 90 -100 *GHz*, as shown in Fig. 8, more details on the design can be referred to in paper [38].

The mode converter employed a single rectangular aperture to couple between the TE_{10} mode in the rectangular waveguide and TE_{11} mode in circular waveguide. The detail of the design can be referred to in [39]. Also to enhance the transmission coefficient, a broadband reflector was designed, optimized and placed at the side towards the electron gun [40].

Tab. 1 Ohmic loss of individual component

Component	Loss (dB)
pillbox window	0.6
waveguide bend	0.4
elliptical polarizers 1	0.9
HCIR	1.5
waveguide taper	1.0
elliptical polarizers 2	0.6
circular-to-rectangular converter	0.3

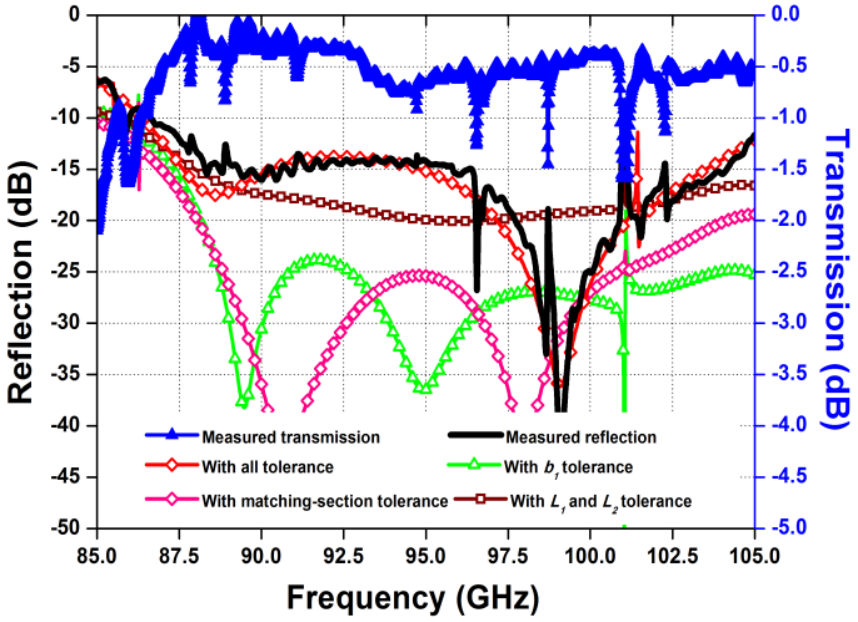

Fig. 8 The simulated and measured results of the pillbox window.

The measurement by a vector network analyzer (VNA) of the whole input coupling system connecting to the beam tube is shown in Fig. 9. A summary of the average loss from each component over the interested frequency range is listed in Table 1. The loss of the input coupling system can, therefore, be obtained. The transmission coefficient of the whole measured circuit is better than -6 *dB* over the interested frequency of 90-100 *GHz*, as shown in Fig. 10. The loss of the whole input coupling system is about -2.0 *dB*, which includes the loss from the pillbox window and the waveguide bends but excludes the loss of the HCIR and the elliptical polarizers.

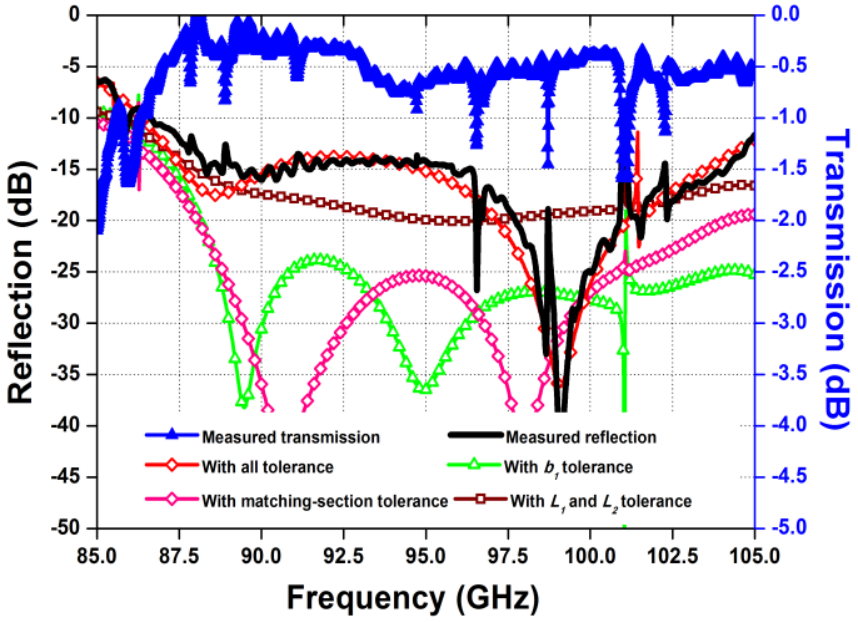

Fig. 9 The connection of the input coupler in the measurement.

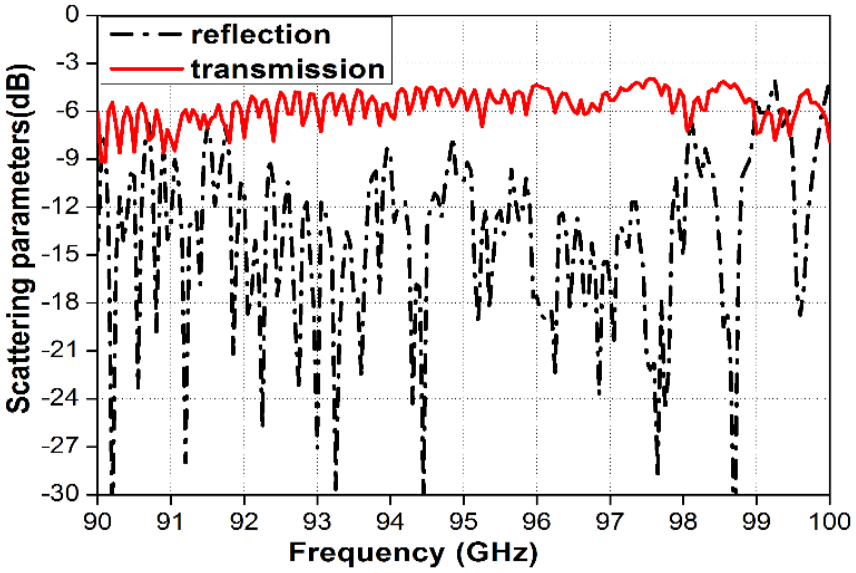

Fig. 10 The measurement setup of the input coupler system at W-band.

(d) Output coupling system

The output coupling system consists of a mode converting horn and a microwave window. At the exit of the HCIR the waveguide mode is the TE_{11}, so the mode converter is used to convert this to the Gaussian-like hybrid HE_{11} mode which is preferred by many applications. There are many choices for this type of mode converter. A corrugated horn was initially designed that achieved excellent conversion efficiency as well as low cross-polarization [41, 42]. However, the drawback of the corrugated horn was its use within the UHV environment. The corrugation vanes will trap a large volume of air, as well as increasing the surface area within the corrugated horn resulting in a much longer time to reduce the vacuum to the required level. A convenient method to solve this issue is to use a smoothly profiled horn [43]. This has the major advantage of being directly machined from solid copper and does not suffer the vacuum issues discussed above. However, this comes with the cost of a reduced Gaussian mode purity, lower gain and reduction in bandwidth.

This configuration had two sections, a non-linear taper, and a linear phase-matching taper. The former taper was designed through an optimization routine with the goal of creating the 85% TE_{11} and 15% TM_{11} mode mixture of the HE_{11} mode. The later taper length was determined through the proper phasing of those modes at its aperture. The input diameter (3.6 *mm*) was pre-determined by the output of the HCIR and the output diameter (25.12 *mm*) was set to be a few times the wavelength diameter so it was large enough for the beam to have a useful far-field profile and as well to assist in the design of the microwave window. Once manufactured the horn was connected to one port of a vector network analyzer (VNA) and allowed to radiate to free space and its reflection was measured, see Fig. 11(a), to be less than -35 *dB*. Afterward, its far-field profile was measured through the VNA, see Fig. 11(b), and showed a good correlation with

the simulations. It was shown to have a directivity of 27 *dB*, side lobes lower than -30 *dB* with a cross-polar level of -25 *dB*.

There are a few types of microwave windows that can be used to couple the microwave radiation out from the ultra-high-vacuum inside the gyro-TWA, for example, the Brewster type, single or multiple disk types, the pillbox type. The Brewster window was designed and measured [44], although it achieved low reflection (~-23 *dB*) and demonstrated a broad bandwidth, it requires an additional polarization converter after the HCIR to convert the circularly polarized output radiation into a linearly polarized one. The window would also be within a corrugated structure which is not preferable for the reasons already discussed.

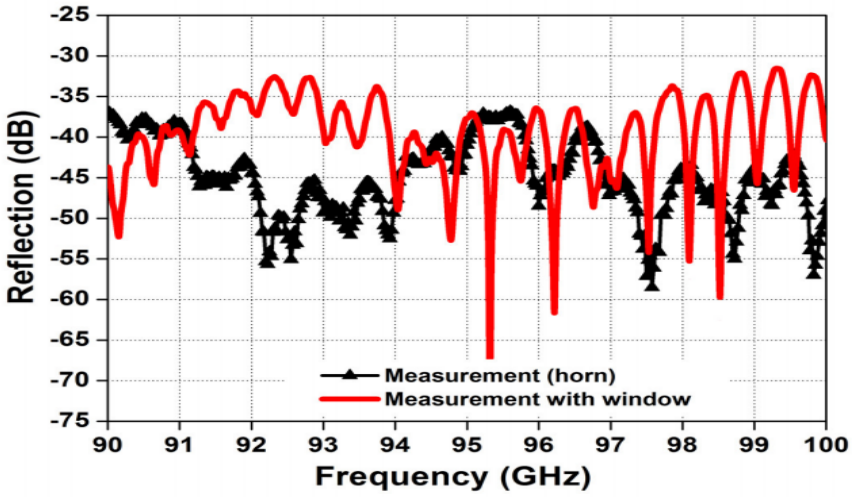

(a)

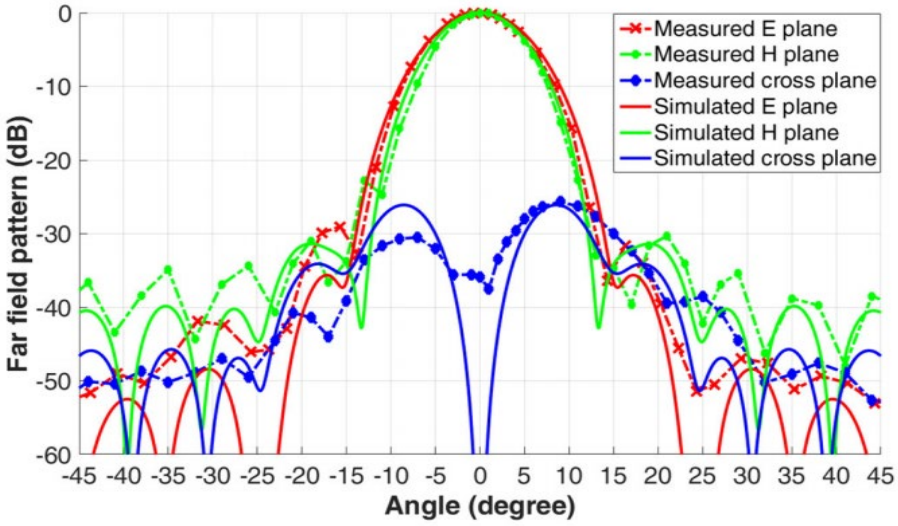

(b)

Fig. 11 The measurement of the smoothly profiled horn including a) its reflection when radiating into space with and without the microwave window and b) the setup of the input coupler system at W-band.

The multiple-layer window was chosen for this output system as it can have very low reflection and wide bandwidth [45, 46]. This configuration consists of different layers of dielectric materials, the more layers the wider the bandwidth but in practice, it is difficult to control those layer's thickness so a trade-off is required. To cover the 10% bandwidth of the gyro-TWA a 5-layer window was suitable. In this case, the central disc was Alumina oxide, Al_2O_3, (97% pure) with relative dielectric constant (ε_r) of 9.4 was used. On each side of it was a small air gap then two thin Quartz discs, with ε_r of 3.75, were placed. The Alumina oxide disc was vacuum brazed into a Titanium holder, which itself had a CF knife edge feature, this held the vacuum to better than 10^{-9} mBar leak rate. The assembled window was placed at the end of a corrugated horn, which converted the input mode to the HE_{11} mode. As there were steps in the window assembly to control the separation distance between the Quartz discs and the central disc, they would cause unwanted reflections so the HE_{11} mode would centrally locate the wave, in order to mitigate this problem. The measurement of the window connected to one port of a vector network analyzer and radiating into free space can be seen in Fig. 12. It showed that over the desired frequency range less than -30 *dB* reflection was achieved, except in one small frequency range, as shown in Fig. 13. After the microwave window was measured and showed, it could achieve the desired reflection level/. It was then connected to the smoothly profiled horn, which had replaced the corrugated type as discussed. The measurement of this assembly of their combined reflection was found and had a lower than -30 *dB* reflection over the whole frequency range. The assembly was then connected to the gyro-TWA experiment, as shown in Fig. 14.

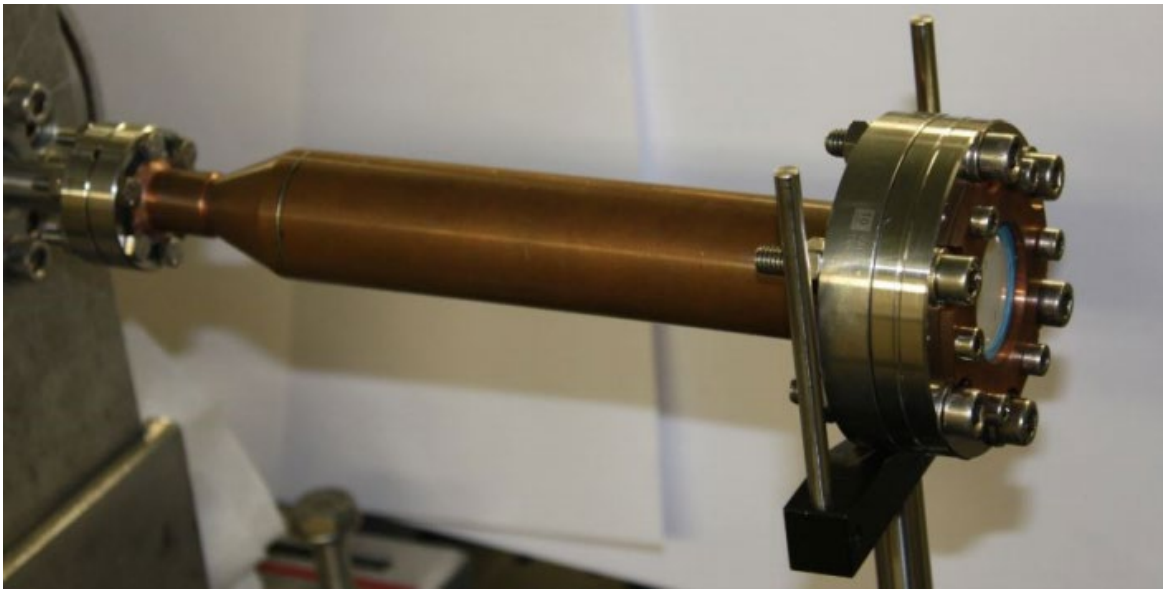

Fig. 12 The smoothly profiled mode converter and microwave window.

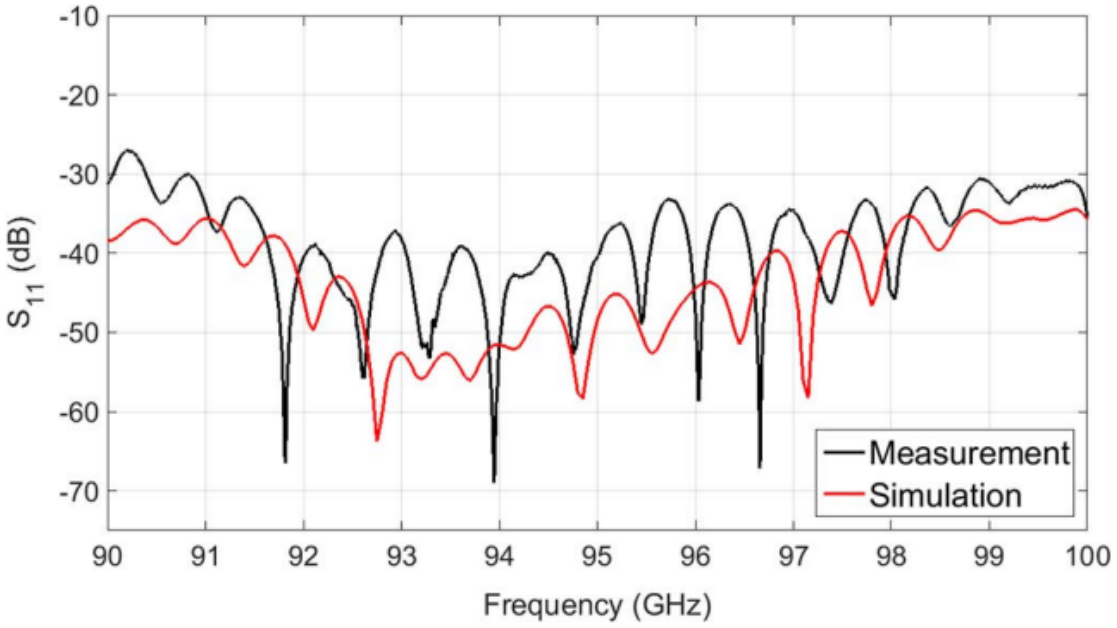

Fig. 13 The measurement of the multilayer microwave window.

3. Prototype and experimental results

After the measurement of the individually designed components presented in the previous section, the W-band gyro-TWA was assembled and the experimental setup is shown in Fig. 14. The solid-state input source was able to generate a maximum power of 1.5 *W* over the frequency range of 90-96 *GHz*. Due to the attenuation of an isolator, a long standard waveguide, and the input coupler, the power that reached the interaction region was about 0.5 *W*. The electron beam energy was accelerated with 55 *kV* at a pulse length of 400 *ns*, generated by a cable pulser. The cusp magnetic field was generated by two water-cooled DC solenoids that were powered by opposite current directions. The maximum magnetic field strength that could be produced under the safe cooling temperature at the maximum driving current from the power supply was 2.1 *T*. The output power of the gyro-TWA was measured by a well-calibrated in-band power meter. The output signal after attenuation from propagating in free space was fed into a mixer with a local oscillator (LO) signal at 94.9 *GHz*. The intermediate frequency (IF) signal was directly captured by a fast digitizing oscilloscope. The measured signal of the beam voltage, beam current, detector signal, as well as the IF signal is shown in Fig. 15.

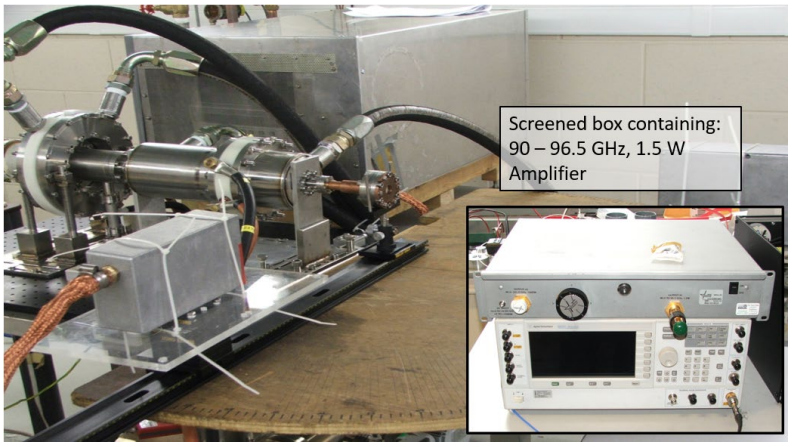

(a)

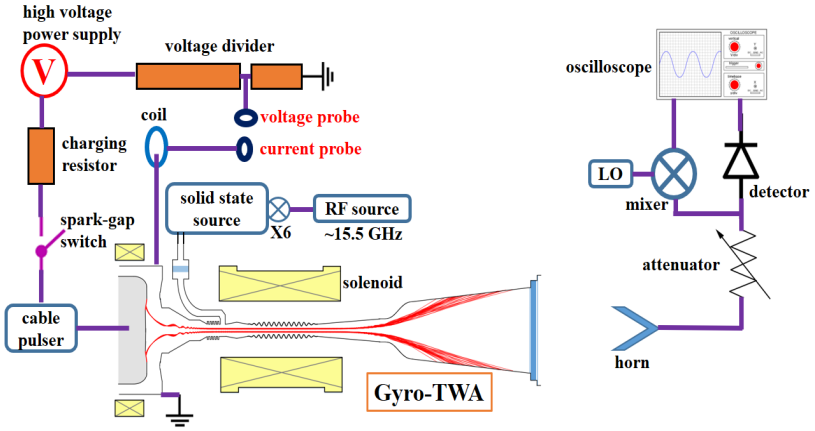

(b)

Fig. 14 The experimental setup (a) and the schematic (b) of the W-band gyro-TWA.

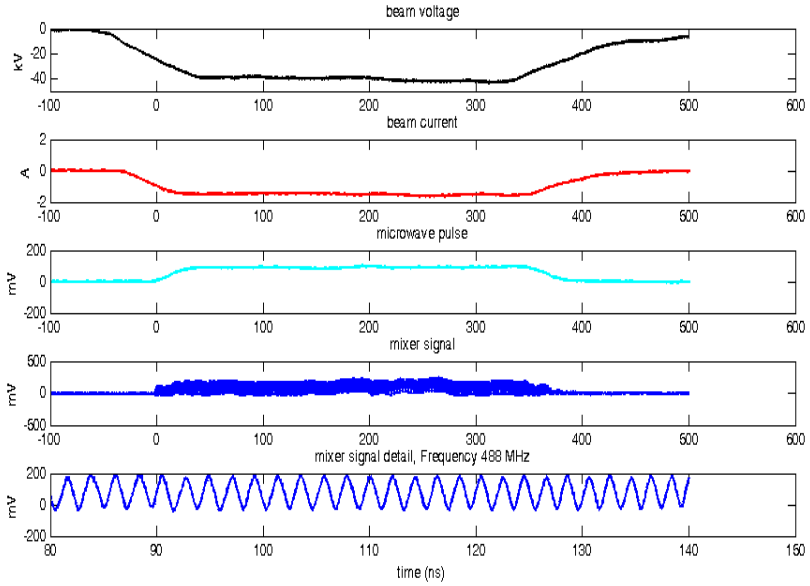

Fig. 15 The measured beam voltage, beam current, detector signal, and the intermediate signal.

The bandwidth of the gyro-TWA in the measurement is 91-96.5 *GHz* with a maximum gain of 38 *dB* at 94 *GHz*. The output power is about 3.4 *kW*. The amplifier was not yet saturated due to a limited input power of the solid-state source. More details on the experiment results can be referred to in paper [7].

The following experiments were carried out after the measurement of the characteristics of the gyro-TWA to evaluate its performance in communication applications. The signal generator, signal acquisition, and data processing package were all from Keysight Technology to provide a complete solution. For example, the arbitrary signal generator Keysight M8190A was used to generate different types of signals, such as a two-tone signal, frequency swept signal, etc. The signal analyzer Keysight PXA N9030A was used to measure the frequency spectrum from the output signal. Due to the lack of a CW high voltage power supply, the experiments could only operate at aburst mode. However, a good phase correlation between the broadband input and output signals, as shown in Fig. 16, was demonstrated. Fig. 16(a) shows the power level of the signal with and without the amplification. Fig. 16(c) is the real-time phase response of the output signal. Fig. 16(b) is the overlay of the frequency response of the input and output signals [47]. Although the noise from the pulsed power supply was evident in the measurement, the gyro-TWA still demonstrated a good phase response.

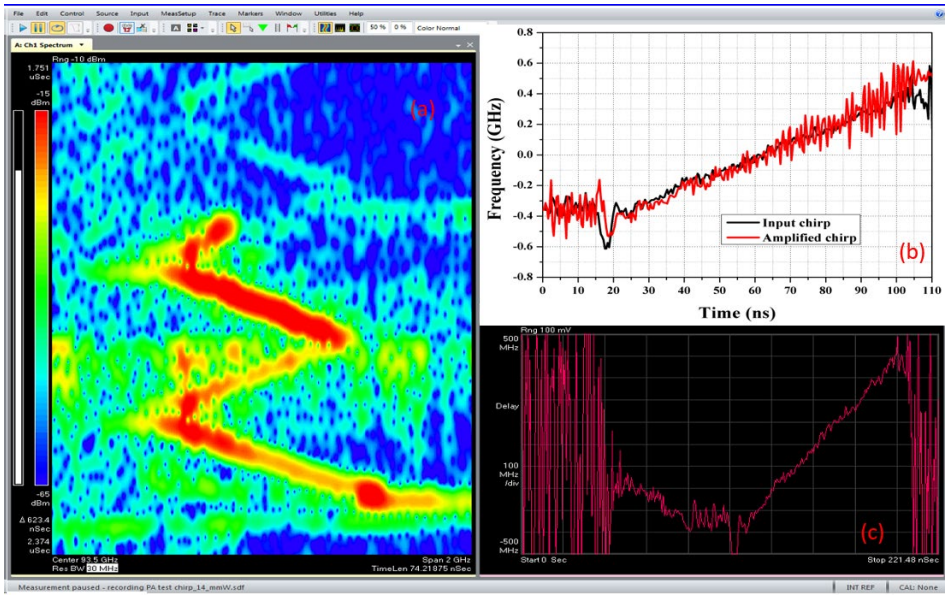

Fig. 16 Measurement of the frequency-swept amplification.

4. Further developments

Two main research areas are being explored based on the success of the previous prototype. One is to operate the W-band gyro-TWA in CW mode, or with a high repetition rate, and the other is the development of gyro-TWAs at higher frequencies.

Although in principle, the prototype is able to operate at a longer pulse length, the cooling requirement of the solenoids is one of the obstacles to achieving this. One of the solutions is to use a superconducting magnet to take the place of the conventional copper-wound solenoids. At the same time, fast switching of the electron beam by employing a modulation electrode is also proposed. Currently, a cusp electron with a modulation electrode has been optimized the match with a newly designed superconducting magnet. A comparison of the geometry of both the cusp electron gun with and without the modulation electrode is shown in Fig. 17. More detail of the design can be referred to in paper [48].

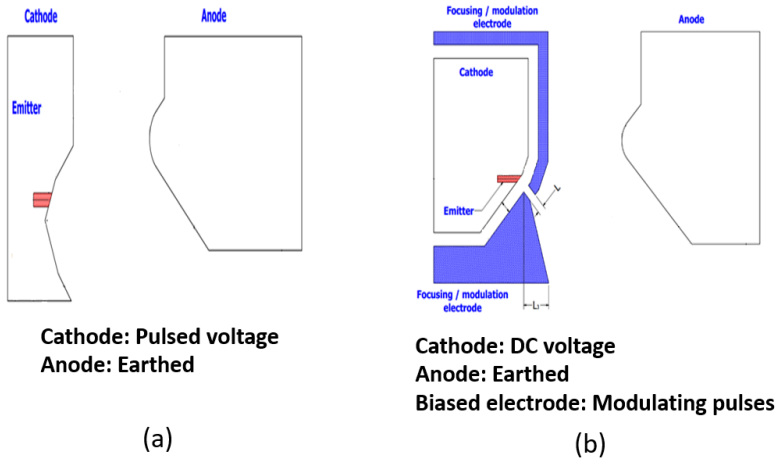

Fig. 17 The cusp electron gun without (a) and with (b) the modulation electrode.

The interaction efficiency of the gyro-TWA is relatively low compared with the conventional TWT and klystron due to the axial energy that does not contribute to the beam-wave interaction. The thermal management becomes increasingly important when it is operating in CW mode. The calculation of the thermal distribution inside the interaction region due to the ohmic loss and the collector due to the spent electrons are required [49]. A depressed collector is a passive converter. It is able to transfer the kinetic energy of the spent electrons into potential electric energy. The overall efficiency is therefore increased and results in less thermal energy deposited on the collector. Based on the previous studies on the depressed collector for X-band gyro-BWO, the research on the depressed collector for the W-band gyro-TWA is carrying on [50, 51].

When the frequency becomes higher, there is increasing difficulty in the manufacture as well as the control of the beam quality due to the smaller dimensions. A major challenge is to

overcome in the realization of the HCIR operating at a higher frequency, for example, a 3-fold at 384 *GHz* was manufactured and tested. The details can be referred to in the paper [52]. Operating at higher-order modes are also proposed to allow the larger structure dimensions and reduce the requirement on the manufacturing. For example, coupled modes TE_{22} and TE_{31} as shown in Fig. 18. when operating at TE_{31} mode, the radius of the five-fold helically corrugated waveguide can be 60% larger than a three one that operates at TE_{21} one, which makes the manufacturing much easier and better surface quality should be achieved [53].

Fig. 18 The field pattern of the hybrid mode TE_{22} and TE_{31} in a five-fold HCIR and the TE_{31} mode in a circular waveguide.

However, operating at higher-order mode makes the design of the input coupler and output windows more challenging, especially as the acceptable geometrical tolerance becomes increasingly tight. Studies on the individual terahertz components, including the multiple-branch terahertz coupler and multiple-layer terahertz window, have been carried out to evaluate their performance and determine the tolerance requirements. The details can be referred to in papers [52, 54, 55].

5. Conclusion

This paper summaries the research work of high-power, broadband millimeter and terahertz wave gyro-TWAs in Strathclyde University. A W-band gyro-TWA has achieved an unsaturated output power of 3.4 *kW* and a gain of 36-38 *dB* in the frequency range of 90-96 *GHz*. A further experiment has demonstrated its potential application in communication. A summary of the design of each component is also presented in this paper. The current on-going following-on researches are also introduced in this paper.

References

[1] K. R. Chu. "The electron cyclotron maser". *Rev. Mod. Phys.,* 76, 2, 489-540 (May. 2004), doi: 10.1103/RevModPhys.76.489.

[2] G. G. Denisov, V. L. Bratman, A. D. R. Phelps, et al. "Gyro-TWT with a helical operating waveguide: new possibilities to enhance efficiency and frequency bandwidth". *IEEE Trans. Plasma Sci.,* 26, 3, 508-518 (1998), doi: 10.1109/27.700785.

[3] W. He, C. R. Donaldson, L. Zhang, et al. "High Power Wideband Gyrotron Backward Wave Oscillator Operating towards the Terahertz Region". *Phys. Rev. Lett.,* 110, 16, 165101 (2013), doi: 10.1103/PhysRevLett.110.165101.

[4] W. He et al. "Theory and simulations of a gyrotron backward wave oscillator using a helical interaction waveguide". *Appl. Phys. Lett.,* 89, 9, 091504 (2006), doi: 10.1063/1.2345607.

[5] G. G. Denisov et al. "Gyrotron Traveling Wave Amplifier with a Helical Interaction Waveguide". *Phys. Rev. Lett.,* 81, 25, 5680-5683 (Dec. 1998), doi: 10.1103/PhysRevLett.81.5680.

[6] V. L. Bratman et al. "High-Gain Wide-Band Gyrotron Traveling Wave Amplifier with a Helically Corrugated Waveguide". *Phys. Rev. Lett.,* 84, 12, 2746-2749 (2000), doi: 10.1103/PhysRevLett.84.2746.

[7] W. He, C. R. Donaldson, L. Zhang, et al. "Broadband Amplification of Low-Terahertz Signals Using Axis-Encircling Electrons in a Helically Corrugated Interaction Region". *Phys. Rev. Lett.,* 119, 18, 184801, (Oct. 2017), doi: 10.1103/PhysRevLett.119.184801.

[8] L. Zhang et al. "Experimental Study of Microwave Pulse Compression Using a Five-Fold Helically Corrugated Waveguide". *IEEE Trans. Microwave TheoryTechn.,*63,3,1090-1096(2015), doi: 10.1109/TMTT.2015.2393882.

[9] S. V. Samsonov et al. "Compression of Frequency-Modulated Pulses using Helically Corrugated Waveguides and Its Potential for Generating Multigigawatt rf Radiation". *Phys. Rev. Lett.,* 92, 11, 118301 (Mar. 2004), doi: 10.1103/PhysRevLett.92.118301.

[10] V. L. Bratman et al. "Generation of 3 GW microwave pulses in X-band from a combination of a relativistic backward-wave oscillator and a helical-waveguide compressor". *Physics of Plasmas,* 17, 11 (Nov 2010), Art no. 110703, doi: 10.1063/1.3505825.

[11] S. V. Kuzikov, A. V. Savilov, and A. A. Vikharev. "Flying radio frequency undulator". *Appl. Phys. Lett.,* 105, 3, 033504, 2014/07/21 (2014), doi: 10.1063/1.4890586.

[12] L. Zhang, W. He, J. Clarke, et al. "Systematic study of a corrugated waveguide as a microwave undulator". *Journal of Synchrotron Radiation,* 26, 1 (2019), doi: doi:10.1107/S1600577518014297.

[13] P.-K. L. Chao-Hai Du. *Millimeter-Wave Gyrotron Traveling-Wave Tube Amplifiers*. Springer, Berlin, Heidelberg (2014).

[14] K. R. Chu et al., "Ultrahigh Gain Gyrotron Traveling Wave Amplifier". *Phys. Rev. Lett.,* 81, 21, 4760-4763 (1998). [Online]. Available: https://link.aps.org/doi/10.1103/PhysRevLett.81.4760.

[15] E. A. Nanni, S. M. Lewis, M. A. Shapiro, et al. "Photonic-Band-Gap Traveling-Wave Gyrotron Amplifier". *Phys. Rev. Lett.,* 111, 23, 235101 (Dec. 2013), doi: 10.1103/PhysRevLett.111.235101.

[16] J. X. Wang et al. "Simulation and Experiment of a Ku-Band Gyro-TWT". *IEEE Trans. Electron Devices,* 61, 6, 1818-1823 (Jun 2014), doi: 10.1109/ted.2013.2296552.

[17] S. V. Samsonov et al., "Ka-Band Gyrotron Traveling-Wave Tubes With the Highest Continuous-Wave and Average Power". *IEEE Trans. Electron Devices,* 61, 12, 4264-4267 (2014), doi: 10.1109/TED.2014.2364623.

[18] S. V. Samsonov et al. "CW Ka-Band Kilowatt-Level Helical-Waveguide Gyro-TWT". *IEEE Trans. Electron Devices,* 59, 8, 2250-2255 (2012), doi: 10.1109/TED.2012.2196703.

[19] S. V. Samsonov, A. A. Bogdashov, G. G. Denisov, et al. "Cascade of Two W-Band Helical-Waveguide Gyro-TWTs With High Gain and Output Power: Concept and Modeling". *IEEE Trans. Electron Devices,* 64, 3, 1305-1309 (2017), doi: 10.1109/TED.2016.2646065.

[20] L. Zhang et al. "Multi-Mode Coupling Wave Theory for Helically Corrugated Waveguide". *IEEE Trans. Microwave Theory Techn.,* 60, 1, 1-7, (Jan 2012), doi: 10.1109/tmtt.2011.2170848.

[21] G. G. Denisov and M. G. Reznikov. "Corrugated cylindrical resonators for short-wavelength relativistic microwave oscillators". *Radiophysics and Quantum Electronics,* 25, 5, 407-413 (May 1982), doi: 10.1007/bf01035315.

[22] S. V. Mishakin and S. V. Samsonov. "Analysis of Dispersion and Losses in Helically Corrugated Metallic Waveguides by 2-D Vector Finite-Element Method". *IEEE Trans. Microwave Theory Techn.,* 59, 9, 2189-2196 (Sept. 2011), doi: 10.1109/TMTT.2011.2160201.

[23] G. Burt et al. "Dispersion of helically corrugated waveguides: Analytical, numerical, and experimental study". *Physical Review E,* 70, 4, 046402 (Oct. 2004), doi: 10.1103/PhysRevE.70.046402.

[24] G. Schmidt. "Nonadiabatic Particle Motion in Axialsymmetric Fields". *The Physics of Fluids,* 5, 8, 994-1002 (1962), doi: 10.1063/1.1706715.

[25] C. H. Du et al. "Development of a Magnetic Cusp Gun for Terahertz Harmonic Gyrodevices". *IEEE Trans. Electron Devices,* 59, 12, 3635-3640 (Dec 2012), doi: 10.1109/ted.2012.2220547.

[26] C. H. Du, X. B. Qi, B. L. Hao, et al. "Conformal Cross-Flow Axis-Encircling Electron Beam for Driving THz Harmonic Gyrotron". *Ieee Electron Device Letters,* 36, 9, 960-962 (Sep 2015), doi: 10.1109/led.2015.2460457.

[27] M. J. Rhee and W. W. Destler. "Relativistic electron dynamics in a cusped magnetic field". *The Physics of Fluids,* 17, 8, 1574-1581 (1974), doi: 10.1063/1.1694936.

[28] W. W. Destler and M. J. Rhee. "Radial and axial compression of a hollow electron beam using an asymmetric magnetic cusp". *The Physics of Fluids,* 20, 9, 1582-1584, 1977/09/01 (1977), doi: 10.1063/1.862029.

[29] D. A. Gallagher, M. Barsanti, F. Scafuri, et al. "High-power cusp gun for harmonic gyro-device applications". *IEEE Trans. Plasma Sci.,* 28, 3, 695-699 (2000), doi: 10.1109/27.887705.

[30] W. W. Destler, R. Kulkarni, C. D. Striffler, et al. "Microwave generation from rotating electron beams in magnetron - type waveguides". *J. Appl. Phys.,* 54, 7, 4152-4162, 1983/07/01 (1983), doi: 10.1063/1.332550.

[31] C. R. Donaldson et al. "Design and Numerical Optimization of a Cusp-Gun-Based Electron Beam for Millimeter-Wave Gyro-Devices". *IEEE Trans. Plasma Sci.,* 37, 11, 2153-2157 (Nov 2009), doi: 10.1109/tps.2009.2031470.

[32] W. L. He et al. *Design, Simulation and Experiment of a Cusp Electron Beam for Millimeter Wave Gyro-devices* (2009 Ieee International Vacuum Electronics Conference). 2009, pp. 517-518.

[33] L. Zhang, W. L. He, C. R. Donaldson, et al. "Investigation on the optimal magnetic field of a cusp electron gun for a W-band gyro-TWA". *Physics of Plasmas,* 25, 5 (May 2018), Art no. 053104, doi: 10.1063/1.5027070.

[34] L. Zhang, W. L. He, C. R. Donaldson, et al. "Design and Measurement of a Broadband Sidewall Coupler for a W-Band Gyro-TWA". *IEEE Trans. Microwave Theory Techn.,* 63, 10, 3183-3190 (Oct 2015), doi: 10.1109/tmtt.2015.2464302.

[35] L. Zhang, W. L. He, C. R. Donaldson, et al. "Bandwidth Study of the Microwave Reflectors with Rectangular Corrugations". *Journal of Infrared Millimeter and Terahertz Waves,* 37, 9, 846-856 (Sep 2016), doi: 10.1007/s10762-016-0280-y.

[36] L. Zhang, C. R. Donaldson, J. Garner, et al. "Input coupling systems for millimetre-wave gyrotron travelling wave amplifiers". *Iet Microwaves Antennas & Propagation,* 12, 11, 1748-1751 (Sep 2018), doi: 10.1049/iet-map.2018.0040.

[37] L. Zhang, C. R. Donaldson, and W. L. He. "Design and measurement of a polarization convertor based on a truncated circular waveguide". *Journal of Physics D-Applied Physics,* 45, 34 (Aug 2012), Art no. 345103, doi: 10.1088/0022-3727/45/34/345103.

[38] L. Zhang, C. R. Donaldson, A. W. Cross, et al. "A pillbox window with impedance matching sections for a W-band gyro-TWA". *IEEE Electron Device Letters,* 1-1 (2018), doi: 10.1109/LED.2018.2834859.

[39] L. Zhang, W. He, C. R. Donaldson, et al. "Design and Measurement of a Broadband Sidewall Coupler for a W-Band Gyro-TWA". *IEEE Trans. Microwave Theory Techn.,* 63, 10, 3183-3190 (Oct. 2015), doi: 10.1109/TMTT.2015.2464302.

[40] L. Zhang, W. He, C. R. Donaldson, et al. "Bandwidth Study of the Microwave Reflectors with Rectangular Corrugations". *Journal of Infrared, Millimeter, and Terahertz Waves,* 37, 9, 846-856 (September 01 2016), doi: 10.1007/s10762-016-0280-y.

[41] P. McElhinney et al. "An Output Coupler for a W-Band High Power Wideband Gyroamplifier". *IEEE Trans. Electron Devices,* 64, 4, 1763-1766 (2017), doi: 10.1109/TED.2017.2660304.

[42] P. McElhinney, C. R. Donaldson, L. Zhang, et al. "A high directivity broadband corrugated horn for W-band gyro-devices". *IEEE Trans. Antennas Propag.,* 61, 3, 1453-1456 (2013), doi: 10.1109/TAP.2012.2228840.

[43] L. Zhang et al. "Optimization and Measurement of a Smoothly Profiled Horn for a W-Band Gyro-TWA". *IEEE Trans. Electron Devices,* 64, 6, 2665-2669 (June 2017), doi: 10.1109/TED.2017.2687949.

[44] Y. Zhang et al. "Design and Measurement of a W-Band Brewster Window". *IEEE Microw. Wireless Compon. Lett.,* 25, 12, 826-828 (Dec. 2015), doi: 10.1109/LMWC.2015.2495110.

[45] C. R. Donaldson, W. He, L. Zhang, et al. "A W-Band Multi-Layer Microwave Window for Pulsed Operation of Gyro-Devices". *IEEE Microw. Wireless Compon. Lett.,* 23, 5, 237-239 (May 2013), doi: 10.1109/LMWC.2013.2251619.

[46] C. R. Donaldson, P. McElhinney, L. Zhang, et al. "Wide-Band HE11 Mode Terahertz Wave Windows for Gyro-Amplifiers". *IEEE Transactions on Terahertz Science and Technology,* 6, 1, 108-112 (Jan 2016), doi: 10.1109/tthz.2015.2495221.

[47] L. Zhang, C. R. Donaldson, P. Cain, et al. "Amplification of frequency-swept signals in a W-band gyrotron travelling wave amplifier". *IEEE Electron Device Letters,* 1-1 (2018), doi: 10.1109/LED.2018.2836868.

[48] L. Zhang, C. R. Donaldson, and W. He. "Optimization of a triode-type cusp electron gun for a W-band gyro-TWA". *Physics of Plasmas,* 25, 4, 043120, 2018/04/01 (2018), doi: 10.1063/1.5028262.

[49] S. V. Mishakin and S. V. Samsonov. "An Approach to Thermal Analysis of Helically Corrugated Waveguide Elements of Vacuum Electron Devices". *IEEE Trans. Microwave Theory Techn.,* 66, 12, 5206-5211 (2018), doi: 10.1109/TMTT.2018.2873362.

[50] L. Zhang, W. He, A. W. Cross, et al. "Design of an Energy Recovery System for a Gyrotron Backward-Wave Oscillator". *IEEE Trans. Plasma Sci.,* 37, 3, 390-394 (2009), doi: 10.1109/TPS.2008.2012108.

[51] L. Zhang, W. L. He, A. W. Cross, et al. "Numerical Optimization of a Multistage Depressed Collector With Secondary Electron Emission for an X-band Gyro-BWO". *IEEE Trans. Plasma Sci.,* 37, 12, 2328-2334 (Dec 2009), doi: 10.1109/tps.2009.2034164.

[52] C. R. Donaldson, L. Zhang, M. Beardsley, et al. "CNC Machined Helically Corrugated Interaction Region for a THz Gyrotron TravelingWave Amplifier". *IEEE Transactions on Terahertz Science and Technology,* 8, 1, 85-89 (Jan 2018), doi: 10.1109/tthz.2017.2778944.

[53] S. V. Mishakin, S. V. Samsonov, and G. G. Denisov. "A Helical-Waveguide Gyro-TWT at the Third Cyclotron Harmonic". *IEEE Trans. Electron Devices,* 62, 10, 3387-3392 (2015), doi: 10.1109/TED.2015.2460265.

[54] J. R. Garner, L. Zhang, C. R. Donaldson, et al. "Design Study of a 372-GHz Higher Order Mode Input Coupler". *IEEE Trans. Electron Devices,* 63, 8, 3284-3290 (Aug 2016), doi: 10.1109/ted.2016.2581314.

[55] J. R. Garner, L. Zhang, C. R. Donaldson, et al. "Design Study of a Fundamental Mode Input Coupler for a 372-GHz Gyro-TWA I: Rectangular-to-Circular Coupling Methods". *IEEE Trans. Electron Devices,* 63, 1, 497-503 (Jan 2016), doi: 10.1109/ted.2015.2501028.